








RESEARCH ARTICLE

The immature *Homo naledi* ilium from the Lesedi Chamber, Rising Star Cave, South Africa

Zachary Cofran^{1,2}  | Caroline VanSickle^{2,3}  | Reynaldo Valenzuela¹ | Daniel García-Martínez^{2,4,5}  | Christopher S. Walker^{2,6}  | John Hawks^{2,7}  | Bernhard Zipfel^{2,8} | Scott A. Williams^{2,8,9,10}  | Lee R. Berger² 

¹Anthropology Department, Vassar College, Poughkeepsie, New York, USA

²Centre for the Exploration of the Deep Human Journey, University of the Witwatersrand, Johannesburg, South Africa

³Department of Anatomy, A.T. Still University, Kirksville College of Osteopathic Medicine, Kirksville, Missouri, USA

⁴Physical Anthropology Unit, Department of Biodiversity, Ecology, and Evolution, Faculty of Biological Sciences, Complutense University of Madrid, Madrid, Spain

⁵Centro Nacional de Investigación sobre la Evolución Humana, Burgos, Spain

⁶Department of Molecular Biomedical Sciences, College of Veterinary Medicine, North Carolina State University, Raleigh, North Carolina, USA

⁷Department of Anthropology, University of Wisconsin, Madison, Wisconsin, USA

⁸Evolutionary Studies Institute, University of the Witwatersrand, Johannesburg, South Africa

⁹Center for the Study of Human Origins, Department of Anthropology, New York University, New York, New York, USA

¹⁰New York Consortium in Evolutionary Primatology, New York, New York, USA

Correspondence

Zachary Cofran, Anthropology Department, Vassar College, 124 Raymond Avenue, Box 42, Poughkeepsie, NY 12604, USA.
Email: zcofran@vassar.edu

Funding information

LRB Foundation for Exploration; Lyda Hill Foundation; National Geographic Society; South African Centre for Excellence in Palaeosciences; South African National Research Foundation; Vassar College

Abstract

Objectives: *Homo naledi* is represented by abundant remains from the Dinaledi Chamber of the Rising Star Cave system in South Africa. While pelvic elements from the Dinaledi Chamber of the cave are fragmentary, a relatively complete ilium (U.W. 102a-138) was recovered from the Lesedi Chamber. We reconstructed and analyzed the Lesedi ilium, providing qualitative descriptions and quantitative assessment of its morphology and developmental state.

Materials and Methods: We compared the Lesedi ilium to remains from the Dinaledi Chamber, other South African hominin fossils, and an ontogenetic series of human ilia. We used the Dinaledi adults as a guide for reconstructing the Lesedi ilium. To assess development of the Lesedi ilium, we compared immature/mature proportional ilium height for fossils and humans. We used 3D geometric morphometrics (GMs) to examine size and shape variation among this sample.

Results: The Lesedi ilium showed incipient development of features expressed in adult *H. naledi* ilia. The proportional height of the Lesedi ilium was within the range of human juveniles between 4–11 years of age. GM analyses showed that the Lesedi ilium had an iliac blade shape similar to those of australopiths and an expanded auricular surface more similar to humans.

Conclusions: The reconstructed Lesedi specimen represents the best preserved ilium of *H. naledi*, confirming the australopith-like iliac blade morphology first hypothesized in adult specimens, and establishing that this anatomy was present early in this species' ontogeny. In contrast to australopiths, the Lesedi ilium displays an enlarged sacroiliac joint, the significance of which requires further investigation.

KEYWORDS

Australopithecus, Dinaledi, Makapansgat, os coxae, pelvis

This is an open access article under the terms of the [Creative Commons Attribution-NonCommercial-NoDerivs](https://creativecommons.org/licenses/by-nc-nd/4.0/) License, which permits use and distribution in any medium, provided the original work is properly cited, the use is non-commercial and no modifications or adaptations are made.

© 2022 The Authors. *American Journal of Biological Anthropology* published by Wiley Periodicals LLC.

1 | INTRODUCTION

Homo naledi lived in South Africa between 241–335 ka (Dirks et al., 2017; Robbins et al., 2021), yet retained many features similar to Early Pleistocene *Australopithecus* and *Homo* (Berger et al., 2015). The pelvic anatomy of *H. naledi* has been described as more comparable to *A. afarensis* and *A. africanus* than to other species of *Homo* (VanSickle et al., 2018). Forty hominin fragments from the Dinaledi Chamber of Rising Star Cave represent the *H. naledi* pelvic region, comprising both adult and immature individuals (Berger et al., 2015; VanSickle et al., 2018). The most complete of these is U.W. 101–1100, a right adult ilium preserving parts of the greater sciatic notch (GSN), arcuate line, iliac blade, and iliac crest. This specimen in particular suggests that *H. naledi* had a flared, flat iliac blade, similar to that of *A. africanus* and morphologically distinct from the ilia known for other species of extinct *Homo* (VanSickle et al., 2018). This contributes to the evidence of diversity of pelvic anatomy within the genus *Homo* (Churchill & VanSickle, 2017). However, in light of the fragmentary Dinaledi Chamber sample, the overall morphology and functional significance of the *H. naledi* ilium remains unclear.

Hominin remains from the Lesedi Chamber of Rising Star Cave (U.W. 102) also represent *H. naledi* (Hawks et al., 2017). Skeletal material comes from three areas within the Chamber designated as U.W. 102a, 102b, and 102c, and it is unclear whether the three areas represent one or several depositional histories. The majority of

skeletal remains in the Lesedi Chamber come from the U.W. 102a excavation area, including the associated partial skeleton designated as LES1. Fragments from at least one immature individual also occur at U.W. 102a, including pieces of long bones, a sacrum fragment, and a partial ilium (Hawks et al., 2017). These remains possibly derive from the same individual as immature craniodental material excavated from the U.W. 102b area, which is approximately 3 m away. Testing this possible association requires a consideration of the ontogenetic stage represented by the remains.

The pelvic remains from area U.W. 102a include an adult right pubis fragment (U.W. 102a–348) that has been provisionally attributed to the LES1 skeleton, an immature sacral element (U.W. 102a–210), and several fragments from an immature right ilium (U.W. 102a–138; Hawks et al., 2017). The pubic and sacral elements preserve very little morphology and are not particularly informative. On the other hand, the associated ilium fragments (Figure 1) represent more of the ilium than what is preserved in any other *H. naledi* fossil. The largest fragment of this ilium was pictured in the description of the Lesedi Chamber material by Hawks et al. (2017), but beyond a basic taxonomic assessment, they did not reconstruct or analyze the specimen.

Here, we present a reconstruction and describe the overall preservation and anatomy of the U.W. 102a–138 ilium. This reconstruction enabled several quantitative analyses. We examined the proportions of the specimen with reference to its developmental stage. We then used 3D geometric morphometric (GM) methods to

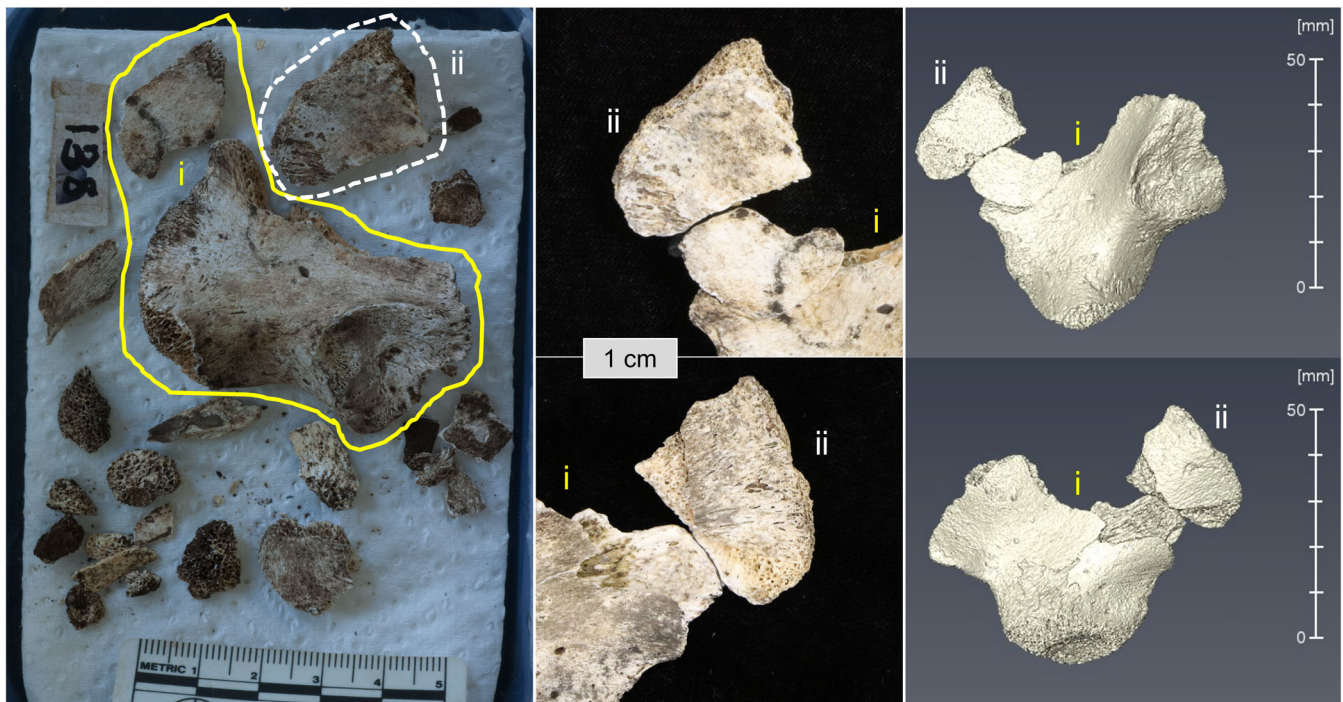


FIGURE 1 Left: Fragments associated with the U.W. 102a–138 ilium. The major fragment (–138i) is circled in yellow, and the iliac crest fragment (–138ii) is circled in a white, dashed line; both are in internal view. Note the small piece within the yellow circle was subsequently refitted and affixed to the major fragment. Center: Photograph of physical arrangement original fragments, focusing on the potential refitting interface, in internal (top) and external (bottom) views. Right: Virtual refitting of the Lesedi ilium fragments, in internal (top) and external (bottom) views

compare the shape of the Lesedi ilium with immature humans and immature *A. africanus* fossils, to test the hypothesis that *H. naledi* retained an overall iliac anatomy similar to that of australopiths. The Lesedi ilium therefore helps address some of the questions about morphology and ontogeny left unanswered by the Dinaledi discoveries.

2 | MATERIALS AND METHODS

2.1 | Comparative collections

Our human sample included 44 ilia from five different skeletal collections (Table 1): two recent samples (Coimbra and the Duckworth anatomy collections from Portugal and England, respectively), a Bronze Age archeological sample (Los Melgarejos, Spain), a Neolithic archeological sample (West Kennet, England), and a single infant from the Mesolithic site of Vela Spila, Croatia. These samples included individuals of different developmental stages (Table 2); chronological age and sex are known for the Coimbra individuals, though these demographic variables are unknown for individuals from the Duckworth anatomy (which are isolated and unassociated with other skeletal or dental elements) and archeological collections. Although this sample is

geographically restricted to Europe, we note that it spans a broad time range, and therefore probably represents a range of activity levels and a diverse set of populations (e.g., Nielsen et al., 2017).

We studied original South African fossil hominin ilia, including U.W. 102a–138, *H. naledi* from the Dinaledi Chamber, juvenile *Australopithecus* specimens MLD 7 (Dart, 1949) and MLD 25 (Dart, 1958), *A. sediba* (MH1; Berger et al., 2010; Kibii et al., 2011; Churchill et al., 2018), *A. africanus* (Sts 14), and SK 3155b, which has an uncertain species designation (Brain et al., 1974). For the GM analysis described below, we limited the fossil comparative sample to MLD 7 and MLD 25, as these immature specimens are well preserved and therefore require minimal reconstruction or incorporation of uncertainty, in comparison with more poorly preserved specimens (i.e., MH1). Moreover, these immature specimens from Makapansgat display the relatively thin and flaring iliac blade characteristic of adult australopiths (Berge, 1998; Berge & Goularas, 2010; Kibii & Clarke, 2003). These two fossils are therefore best situated to help test the hypothesis that the immature *H. naledi* ilium from Lesedi retained an australopith-like anatomy.

All human ilia, U.W. 102a–138, Dinaledi adult U.W. 101–1100, and most other hominin fossils were digitized using an Artec Spider surface scanner and processed into 3D surface meshes using Artec Studio software (Artec 3D). Other Dinaledi specimens were previously

TABLE 1 Number of individuals from each skeletal collection in each maturation stage used in this study

Collection	Stage 1 (Infant)	Stage 2 (Juvenile)	Stage 3 (Subadult)	Stage 4 (Adult)	Total
Coimbra	0	6	4	0	10
Duckworth	2	4	0	6	12
Los Melgarejos	1	2	2	3	8
West Kennet	2	6	1	4	13
Vela Spila	1	0	0	0	1
Total	6	18	7	13	44

TABLE 2 Description of developmental stages

Stage	Age group	Age range (years)	Description
1	Infant	<4	All epiphyses are unfused. Acetabulum and AIIS surfaces are smooth. There is a weak demarcation between the articular surfaces for the ischial and pubic secondary ossification centers (posterior epiphysis and os acetabuli).
2	Juvenile	4–11	All epiphyses are unfused. Acetabulum and AIIS surfaces are becoming billowed and more complex. The secondary ossification centers at the pubis (os acetabuli) and ischium (posterior epiphysis) may be forming but are not yet fused with the primary ossification center.
3	Subadult	12–22	Acetabulum has started to fuse with secondary ossification centers (os acetabuli and posterior epiphysis), but fusion is not yet complete. The secondary ossification centers at the AIIS (superior epiphysis) and the iliac crest (anterior and posterior epiphyses) have started to ossify and fuse.
4	Adult	>22	Acetabulum, AIIS, and iliac crest have all fully fused.

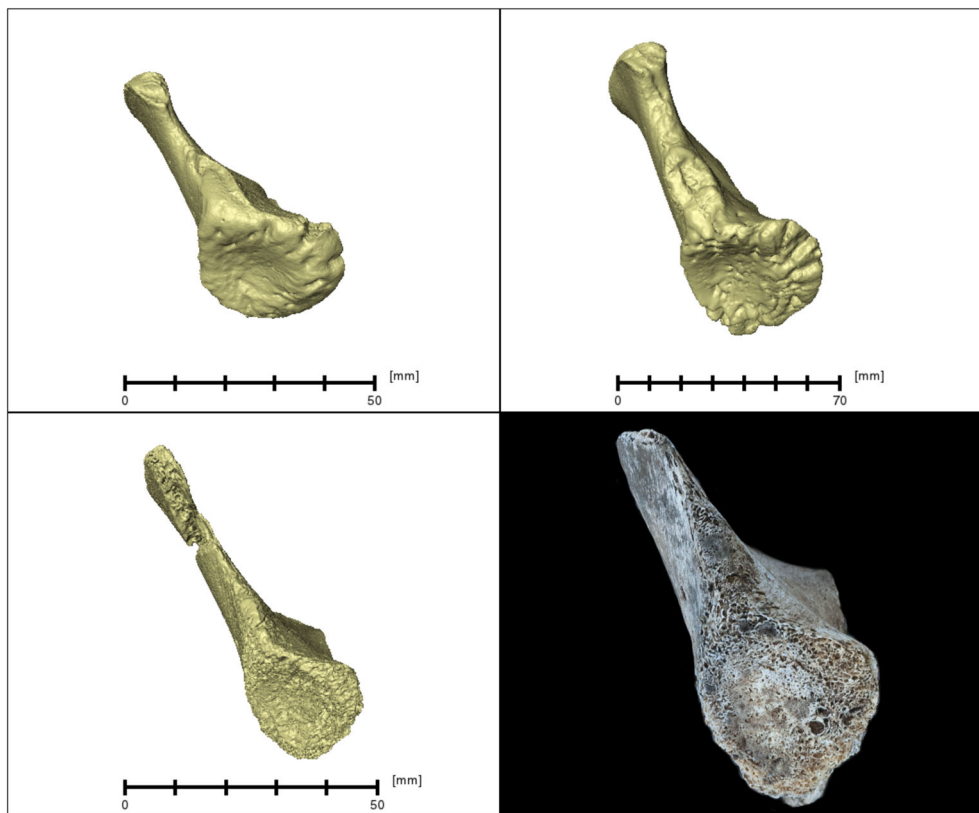


FIGURE 2 Examples of acetabulum and anterior inferior iliac spine of humans in Stage 1 (top left) and Stage 2 (top right). The Lesedi ilium is depicted as both a surface mesh (bottom left) and close-up original photograph (bottom right). Note that left and right panels are at different scales, and the Lesedi mesh and photograph are at slightly different perspectives

digitized with a NextEngine 3D laser scanner, and were included for visual comparisons only. Most individuals are represented by the right side, but where preservation was best on the left, these meshes (including MLD 7 and MLD 25) were mirror-imaged prior to analysis.

We seriated ilia into four developmental stages based on the development of the acetabulum (Figure 2), using standards from Scheuer and Black (2000; Table 2). In support of our seriation, Coimbra individuals assessed as Stage 2 range from 10 to 12 years old, while those in Stage 3 are 16 years of age. In addition, the Vela Spila individual, assessed as Stage 1, was previously estimated to have died around 2–3 years of age based on skeletal and dental development (Radović et al., 2018). Thus, all individuals for whom chronological age was known (Coimbra) or estimated across the skeleton (Vela Spila) were consistent with the ilium stage seriation. The archeological remains from Los Melgarejos and West Kennet are largely commingled and mostly lack association with other skeletal elements, but where associations are apparent, the other elements are developmentally consistent with our assessments of ilium maturation.

2.2 | Initial preparation of the Lesedi ilium

There are multiple iliac fragments from Lesedi numbered U.W. 102a–138 (Figure 1). The largest fragment, which we will call U.W. 102a–138i, was described by Hawks et al. (2017). It preserves the auricular surface, a partial iliac blade, the arcuate line, most of the GSN, the anterior inferior iliac spine (AIIS), and the iliac portion of the unfused acetabulum. The second largest fragment, U.W. 102a–138ii, has not

previously been described. This fragment measures 18.9×25.7 mm, and includes the anterior part of the iliac crest and abraded surfaces of the cristal tubercle and anterior superior iliac spine (ASIS) (Figures 1 and 3).

Although we are confident in our identification of the 138ii fragment, it was nevertheless unclear precisely how it articulates with the larger 138i fragment, as the only contact is a thin segment of cortical bone on the iliac surface. This break is fairly straight and slight contours on each piece suggest a probable contact between fragments (center panel in Figure 1). Our hypothesized refitting of these fragments was based on (1) the subtle morphology of the break, (2) the smooth contour of the iliac surface across the two pieces, and (3) the alignment of the thick and convex gluteal surfaces. This configuration has a continuous acetabulocristal buttress (Figure 3), similar to the mature U.W. 101–1100 ilium from Dinaledi (Figure 4). This reconstruction results in a “two-pillar” morphology, with thicknesses corresponding to both the acetabulocristal and acetabulospinous buttresses. The same morphology is also manifest in the mature U.W. 101–477 fragment; the area of the acetabulospinous buttress is missing in U.W. 101–1100 (Figure 4). Thus, while we acknowledge uncertainties in our reconstruction, we contend that it is reasonable given the state of preservation and the comparative evidence from Dinaledi.

2.3 | Analysis 1: Development

The acetabulum surface of the Lesedi ilium is abraded, confounding its assignment to a developmental stage (i.e., Stages 1–2; Figure 2).

FIGURE 3 Anatomical features of the Lesedi ilium. The larger U.W. 102a–138i fragment is depicted in green and the smaller –138ii fragment in blue. Left: External aspect. Right: Internal aspect

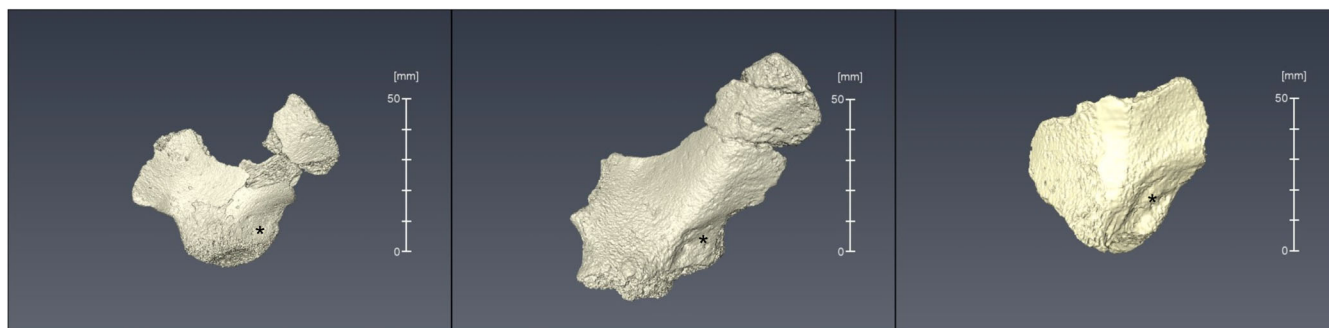
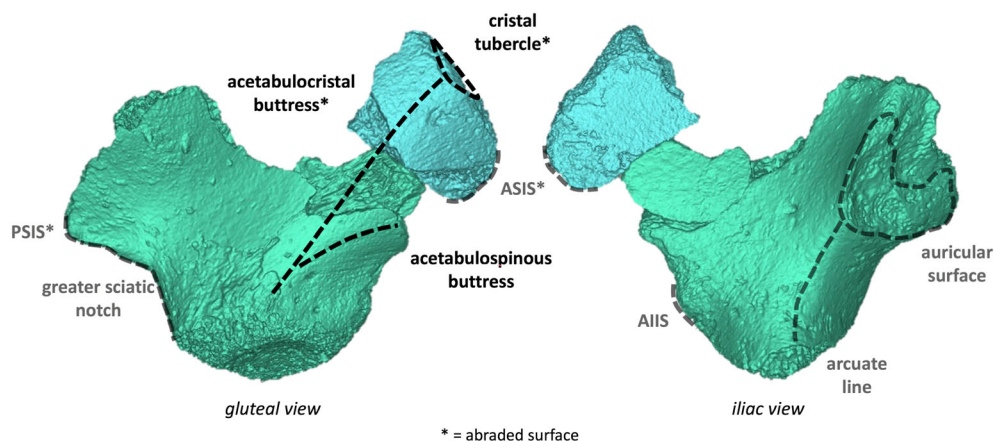


FIGURE 4 External view of the reconstructed Lesedi ilium (left), U.W. 101–1100 (center), and U.W. 101–477 (right). Note the depression (*) beneath the buttresses in each specimen. Images are to scale

Preservation of the Lesedi ilium (as well as Dinaledi specimens) limits the number of traditional linear measurements that can be compared, as most of these involve the full iliac crest and posterior superior iliac spine (PSIS; e.g., Fazekas & Kósa, 1978; Rissech & Malgosa, 2005), neither of which is preserved in Lesedi. However, both the reconstructed Lesedi ilium and the mature Dinaledi specimen U.W. 101–1100 preserve iliac height, measured as the distance from the deepest point of the GSN to the lateral margin of the iliac crest at the presumptive cristal tubercle. We measured iliac height digitally on 3D models of *H. naledi* and modern human ilia using the open-source software Meshlab (Cignoni et al., 2008).

We also measured iliac height in MLD 7, MLD 25, and Sts 14, all generally attributed to *A. africanus* (see Grine, 2013 for discussion of taxonomy). Sts 14 is thought to be a young adult female, with the iliac crest still in the process of fusing (Berge & Goullaras, 2010; Bonmatí et al., 2008). The right ilium of Sts 14 is missing the anterior crest including the ASIS, and so this iliac height (82.76 mm) is likely a slight underestimate since we measured at the break. The left side of Sts 14 preserves more of the iliac crest, but the blade was broken away from the rest of the innominate *post mortem*, and these two components are misaligned and fixed in plaster (Kibii & Clarke, 2003). The left iliac crest lacks a pronounced thickening or cristal tubercle, and so its iliac height at the most lateral point (89.6 mm) is tentative. In light of these uncertainties surrounding Sts 14, we used the average of the two sides, and interpret its iliac height cautiously.

To assess ontogenetic development, we created a proportional size ratio for immature ilia, calculated as the iliac height of the immature individual divided by that of an adult. For the *H. naledi* ilia, we used the Lesedi ilium as the immature individual and U.W. 101–1100 as the adult. For the humans, we used resampling to randomly select an immature individual (Stage 1, 2, or 3) and an adult (Stage 4) to calculate the ratio, and repeated this procedure 2000 times. We compared the resulting ratios for each immature human developmental stage with the ratio calculated for *H. naledi* to estimate its stage of development.

2.4 | Analysis 2: Shape

To examine the shape affinities of the Lesedi ilium, we performed three-dimensional landmark-based GM analyses, including only immature ilia with the acetabulum completely unfused for humans ($n = 23$) and MLD 7 and MLD 25 (*A. africanus*). We first digitized a template of 148 landmarks on a human ilium (Figure 5), using Viewbox 4 software (Halazonetis, 2013) and following the protocol established by Bastir et al. (2019). The landmark template (Table 3) includes eight fixed landmarks, 50 sliding surface semilandmarks distributed across each the internal and external surfaces of the iliac blade, and 40 sliding semilandmarks distributed across four curves corresponding to: (1–2) the lateral and medial margins of the iliac

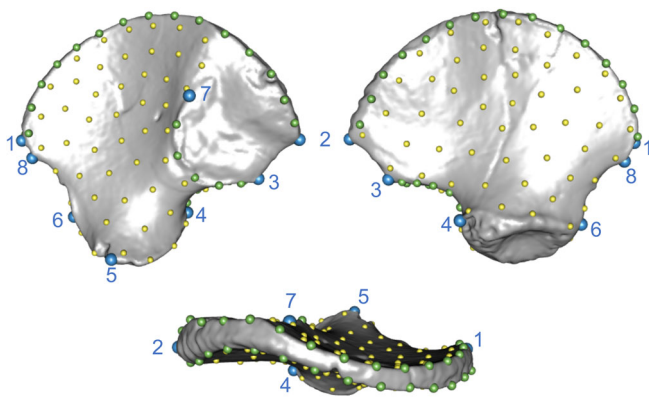


FIGURE 5 Landmark template applied to a human infant. Views clockwise from left: Internal, external, and superior (anterior to right). Large blue spheres represent fixed landmarks, medium green spheres are curve semilandmarks, and small yellow spheres are surface semilandmarks. Numbers correspond with landmarks described in Table 3

crest between the PSIS and anterior crest (Landmarks 2 and 8), (3) the antero-inferior border of the auricular surface between the posterior inferior iliac spine (PIIS) and superior auricular point (Landmarks 3 and 7), and (4) the GSN between the PIIS and ilioischial point (Landmarks 3 and 4). We did not measure landmarks on the auricular surface, iliac tuberosity, or acetabular surfaces as these areas are often damaged or missing in both fossil and archeological remains.

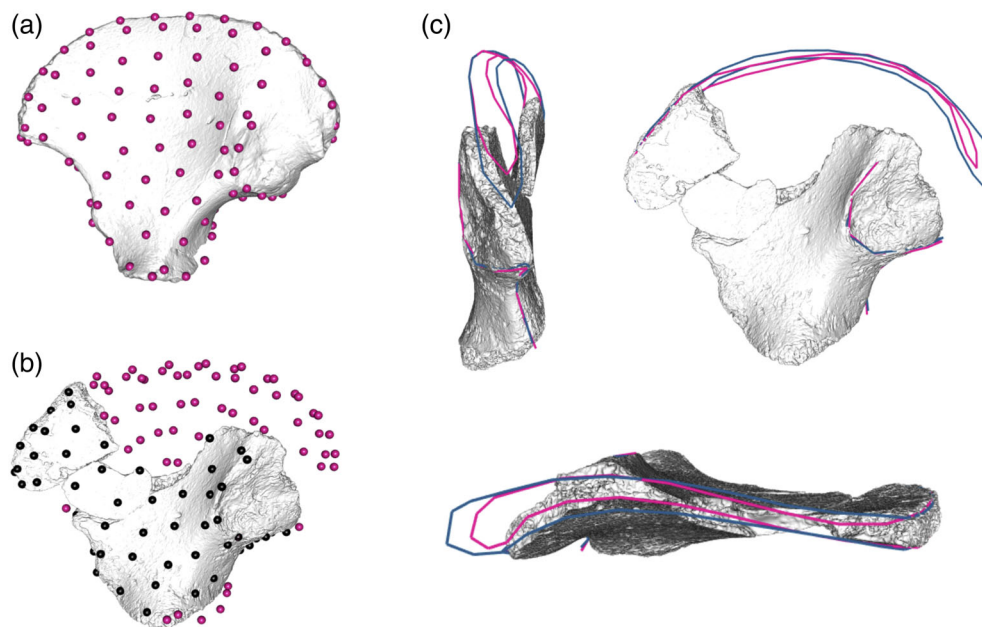
We applied this landmark template to all 23 humans in Stages 1–2, to MLD 7 and MLD 25, and to the Lesedi ilium using Viewbox. In the case of missing landmarks in the comparative sample, these coordinates were estimated using the thin plate spline (TPS) interpolation, minimizing the bending energy between the estimated configuration and the template (Bastir et al., 2019; Gunz et al., 2005; Gunz & Mitteroecker, 2013). As MLD 25 is missing a central portion of the iliac crest and blade, missing landmarks were estimated using MLD 7 as the reference template. MLD 7 is an ideal reference for the missing data of MLD 25, because both are from the same site and stratigraphic unit, are probably of a similar geological age, presumably

TABLE 3 Ilium landmark descriptions

Number	Name	Type	Description
1	ASIS	Fixed	Anterior superior iliac spine; most projecting point at the anterolateral end of the iliac crest
2	PSIS	Fixed	Posterior superior iliac spine; most projecting point at the posteromedial end of the iliac crest
3	PIIS	Fixed	Posterior inferior iliac spine; most posterior extent of the auricular surface at end of the greater sciatic notch
4	Ilioischium	Fixed	Inferior terminus of the greater sciatic notch; posterior-most end of the ilio-ischial junction
5	Iliopubic	Fixed	Anterior terminus of the arcuate line; anteromedial ilio-pubic junction
6	AIS	Fixed	Apex or center of the anterior-inferior iliac spine epiphyseal surface
7	Auricular	Fixed	Superior extent of the auricular surface at the interface of iliac and sacroiliac surfaces
8	Anterior crest	Fixed	Anterior terminus of the iliac crest where medial and lateral margins meet
9–58	Iliac surface (50)	Surface	Sliding semilandmarks distributed across the iliac fossa and subarcuate surface
59–108	Gluteal surface (50)	Surface	Sliding semilandmarks distributed across the the gluteal surface
109–123	Lateral crest (15)	Curve	Sliding semilandmarks along the external margin of the iliac crest, from LM 8 to LM 2
124–128	Auricular (5)	Curve	Sliding semilandmarks along the anterior and inferior margin of the auricular surface, from LM 7 to LM 3
129–133	GSN (5)	Curve	Sliding semilandmarks along the greater sciatic notch, separating the medial from lateral ilium surfaces, from LM 3 to LM 4
134–148	Medial crest (15)	Curve	Sliding semilandmarks along the internal margin of the iliac crest, from LM 8 to LM 2

Note: Numbers in parentheses next to surface and curve names indicate the number of semilandmarks. Abbreviation: LM, fixed landmark numbers.

FIGURE 6 Landmark estimation and reconstruction of the Lesedi ilium. (a) MLD 7 (left, reversed) with the landmark template. (b) The Lesedi ilium with preserved landmarks in black and those estimated from the australopith template in pink. (c) Comparison of reconstructed landmark curves using australopith (pink) and human (navy) templates. Images not to scale



belong to the same species, and are of a similar overall size and developmental stage (Dart, 1958).

After applying the landmark template to each individual and estimating missing data, we used generalized Procrustes analysis (GPA) to obtain the mean or consensus landmark configuration of the entire sample (23 humans, two australopiths, and the Lesedi ilium). We then used this consensus configuration as a template, and reslid all semilandmarks of each individual to minimize the TPS bending energy against this new template (Bastir et al., 2019). This step is important for minimizing differences between landmark configurations, as the individual used for the original template and its semilandmark positions are arbitrary, and may exaggerate shape differences between individuals (Gunz & Mitteroecker, 2013).

Estimating missing data for the Lesedi ilium involved several steps. We first placed the four fixed landmarks that are sufficiently preserved (Landmarks 1 and 6–8), but we had to estimate the positions of the ilioischial and iliopubic junctions (Landmarks 4–5), and the abraded PIIS (Landmark 3). The positions of these landmarks were first mathematically estimated using TPS interpolation in Viewbox, and then manually adjusted based on the preserved morphology of the specimen. In the case of some landmarks and semilandmarks, we allowed points to adhere to abraded surfaces where abrasion was deemed minimal and therefore unlikely to strongly impact the overall results. The PSIS (Landmark 2) was missing entirely and had to be estimated from the TPS interpolation.

We generated two landmark reconstructions for the Lesedi ilium, using either the (reslid) consensus template or MLD 7 as a reference. We first estimated the positions of sliding semilandmarks on preserved surfaces using either template in Viewbox (Figure 6). These reconstructions differ slightly in the positions of some semilandmarks on preserved surfaces, due to differences in ilium shape that are quantified in fixed landmarks and curve semilandmarks, but the differences are not pronounced. To reconstruct the missing iliac blade, we

imported the landmark data from the preserved surfaces into the R computing environment (R Core Team, 2020) and declared all (semi) landmarks on missing surfaces as “NA.” We then used the “fixLMtps” function in the package *Morpho* (Schlager, 2017) to estimate these missing landmarks based on (1) the consensus configuration of the 23 humans, and (2) the MLD 7 and MLD 25 consensus configuration. Comparison of these two reconstructions, with and without the missing landmarks, is presented in the Supporting Information (S1–2).

To examine shape variation, we performed GPA and then principal component analysis (PCA) of the Procrustes-aligned data (Zelditch et al., 2012). GM analyses were performed in R (R Core Team, 2020), using the packages *Geomorph* (Adams et al., 2020), *Morpho* (Schlager, 2017), and *abind* (Plate & Heiberger, 2016). To facilitate visualization of shape variation, we warped the 3D surface mesh of the human ilium closest to the overall sample consensus (“Vela Spila B”), to specific landmark configurations (Bastir et al., 2019; Weber & Bookstein, 2011): the positive and negative extremes of shape space PC1, as well as the reconstructed Lesedi ilium landmarks. Warping was performed using the “warpRefMesh” function of the *Geomorph* package (Adams et al., 2020).

In order to assess potential effects of intraobserver error in landmark placement, we randomly selected three individuals from the human sample to digitize two additional times in Viewbox. Triplicates were digitized at least 24 h apart from one another. Intraobserver error could arise during the placement of both fixed landmarks and the semilandmark curves; sliding of the surface semilandmarks is further influenced by these first two steps. Thus, we examined variation among triplicates for both the eight fixed landmarks alone, and for the full set of 148 landmarks and sliding semilandmarks. In each of these two cases (only eight fixed, or all 148), we subjected the dataset to GPA and compared the Procrustes distances (PD) between the triplicates and all other individuals in the human sample (cf. Rosas et al., 2017); we specifically tested the null expectation that PD would

be lower within a set of triplicates, than between the set and all other individuals in the sample.

PD among sets of triplicates were extremely low compared with the distribution for all pairwise comparisons, for both the eight fixed landmarks alone and the full set of landmarks and semilandmarks (Supporting Information S3). Importantly, we met the null expectation that PDs among triplicate sets would be lower than between each set and all other individuals. Thus, intraobserver error is sufficiently low in the preliminary step of placing fixed landmarks, and it remains low throughout the digitization process so that intraindividual variation remains minimal after the full landmark set is digitized. We are therefore confident that intraobserver error is so miniscule as to have a negligible impact on our results.

2.5 | Analysis 3: Auricular size

Post hoc inspection of the Procrustes-aligned data suggested that the Lesedi ilium was more similar to humans than to australopiths in terms of the size of the sacroiliac joint. To test this inference, we measured the length of the anterior–inferior margin of the auricular surface, as the sum of the interlandmark distances along this curve between Landmarks 3 and 7 (PIIS and superior auricular point). Interlandmark distances were calculated using the function “interlmdist” in the R package *Geomorph* (Adams et al., 2020). We then compared this auricular margin length against two measures of ilium size. The first is the natural logarithm of centroid size, Ln(CS), measuring the overall size of the 3D landmark configuration; this only includes the humans, the Lesedi ilium, and Makapansgat australopiths included in the GM analysis. Because Ln(CS) entails extensive missing data estimation for Lesedi, the second size measurement we used was lower iliac width, which is preserved in the Lesedi ilium with only minor estimation. We measured lower iliac width as the linear distance between AIIS and PIIS (Landmarks 3 and 6), using the “interlmdist” function.

To incorporate relevant fossil hominins that are too incomplete to be included in the GM analysis, we measured the auricular margin length and lower iliac width in MH1, Sts 14, and SK 3155b. Each of these fossils was complete enough to reliably measure these variables, and is skeletally subadult like Lesedi and the rest of our comparative samples (Berge & Gommery, 1999; Bonmatí et al., 2008; Brain et al., 1974). We calculated auricular margin length and lower iliac width by manually placing landmarks comparable to those used in the GM analysis, using the “Measure” function in Artec Studio. Each fossil was measured three times and the average of these measurements was used for analysis. Validating this method, we used it to remeasure the auricular margin length of MLD 7 and a human infant, which yielded measurements very similar to those obtained using the GM approach (1.25 and 0.73 mm different, respectively). By plotting auricular margin length against these two measures of ilium size, we could test whether the Lesedi ilium and other fossil hominins deviated from expectations based on human ontogenetic scaling.

3 | RESULTS

3.1 | Description and comparison of reconstruction

The maximum dimensions of the reconstructed fossil are 67.8 mm from the abraded PIIS to the ASIS, and 62.3 mm from the posterior end of the preserved iliac crest to the abraded iliopubic promontory. The iliac crest is preserved from the ASIS for 25.3 mm, and the entire immature acetabular surface is mildly abraded. The acetabulocrystal buttress is readily apparent but faintly expressed, reaching a maximum thickness of 6.1 mm. The termination of the faint acetabulocrystal buttress at the iliac crest does not form a prominent crystal tubercle, but rather forms a rather blunt curvature maximum; this is similar to U.W. 101–1100 from Dinaledi and MLD 25, and unlike the uniformly flat blade of MLD 7. The presence of the buttress gives this portion of the blade a smooth, convex gluteal or lateral surface, in contrast to the relatively flat iliac or medial surface. The inferior aspect of the gluteal surface shares the crest's convexity, with a palpable thickening for an acetabulocrystal buttress at the anterior edge of the break. Between the thickened buttress posteriorly, AIIS anteriorly, and acetabular margin inferiorly, is a concavity or depression (Figure 4). This depression does not form a shelf-like appearance at the acetabular margin as has been described for the genus *Homo* (e.g., Simpson et al., 2008; Ward et al., 2015) and *A. sediba* (Churchill et al., 2018; Kibii et al., 2011), but the same is true of immature human ilia.

Posterior to the inferior “base” of the buttress, the gluteal surface is relatively flat and missing the thin (<1 mm), outermost layer of cortical bone inferiorly. Posterior to the flat gluteal fossa is a blunt thickening toward the posterior end of the GSN, likely marking the posteroinferior extent of the anterior gluteal line (Scheuer & Black, 2000). The gluteal surface is marked with nutrient foramina, including a large one at the base of the acetabulocrystal buttress anteriorly, and two large ones in the gluteal fossa, the anterior of which may approximate the anterior gluteal line (Scheuer & Black, 2000); other than this foramen and the aforementioned thickening, there is no other discernible development of gluteal lines.

Inferiorly, the immature acetabulum is abraded on all margins (Figure 2), especially posteriorly. Damage is only minor centrally, leaving an ovoid area of well-preserved surface measuring 15.2 mm anteroposteriorly by 8.6 mm mediolaterally. There are a few small patches of unabraded immature surface on the posterolateral edge of this region, and two concavities of this complex metaphyseal surface are also preserved at the anterior end immediately inferior to the AIIS. This acetabular surface is gently concave in all directions.

The GSN measures 22.7 mm from the posteroinferior border of the auricular margins (approximating the PIIS) to the posterosuperior margin of the acetabular surface (approximating the ilioischial junction). The anterior and posterior arms of the notch are relatively straight and set at an obtuse angle to one another, similar to younger humans. Damage to the posterior end of the GSN barely includes the PIIS, which was probably only a few millimeters away from the break.

Moving medially, the majority of the auricular surface is present and well-preserved. Both the cranial and caudal arms of the surface are straight and oblong, oriented roughly perpendicular to one another. Maximum dimensions of these auricular segments are 24.6 mm anteroposteriorly and 16.9 mm superoinferiorly. The auricular surface is abraded, yet intact surfaces, darker than the rest of the bone, are present in the cranial arm and the posterior half of the caudal arm. The anterior rim of the auricular surface is anteroposteriorly convex, and is sharply delineated from the iliac and subarcuate surfaces anteriorly. At its thickest, the posterior ilium at the auricular surface is about 7.1 mm. Between the cranial and caudal arms of the auricular surface, only a small amount of the retroauricular area is preserved.

Anterior to the auricular surface, the acetabulosacral buttress is robust (relative to the diminutive size of the specimen), measuring approximately 10–11 mm thick. The arcuate line is not well delineated but, rather, there is a smooth transition from the subarcuate surface of the true pelvis to the iliac surface of the false pelvis. The subarcuate surface is relatively flat and nearly coplanar with the auricular surface. The subarcuate surface broadens inferiorly; superiorly, the minimum distance between the GSN and the arcuate line is 12.9 mm, while the same measurement inferiorly at the end of the preserved bone at the iliopubic promontory is 17.3 mm. The posterior surface of the iliac fossa near the auricular surface is mildly concave. Anteroinferiorly, the convexity of the iliac surface at the iliopubic promontory grades into the iliopectoral groove at the inferomedial edge of the AIIS. The remainder of the iliac surface is relatively flat and featureless, aside from the large nutrient foramen for a branch of the iliofemoral artery that is 8.4 mm anterior to the auricular surface.

The Lesedi ilium compares favorably with homologues identified in the Dinaledi Chamber, although most of these are consistent with an adult developmental stage (VanSickle et al., 2018). As noted above, the weak cristal tubercle and acetabulocristal/-spinous buttress are similar to U.W. 101-477, -986, and -1100. In all of these individuals, there is a marked concavity anterior to the inferior “base” of the buttress (Figure 4). This same concavity is present in the Lesedi ilium but is less pronounced than in the Dinaledi specimens. We suggest this may be a feature that became more accentuated during ontogeny. On the internal aspect, the iliac fossa surface is not angled as sharply (e.g., “flaring”) relative to the subarcuate surface as in U.W. 101-986 or -1100, in which the angle between these surfaces is nearly perpendicular. Anteriorly, inferomedial to the AIIS, the iliopectoral groove is about equally concave or excavated as in the larger and presumably mature U.W. 101-477, the only Dinaledi specimen preserving this feature. The weakly developed AIIS of the Lesedi ilium appears to angle only slightly relative to the anterior margin of the iliac blade, whereas the AIIS is more strongly flexed or angled, where it is preserved, in U.W. 101-477. In addition, it had previously been suggested that U.W. 101-486, a fragment of the acetabulosacral buttress with some of the anterior-inferior auricular margin, was immature based on its small size (Hawks et al., 2017; VanSickle et al., 2018). Where U.W. 101-486 can be compared with the Lesedi ilium, the former is thicker in the vicinity of the auricular surface and

its iliac body would have been taller (i.e., toward the ilio-ischial junction) compared with Lesedi. While it still cannot be determined whether U.W. 101-486 was immature, at the very least it would have come from a slightly larger, and possibly older, individual than U.W. 102a-138.

In sum, the distinctive morphology of the subarcuate surface and anterior iliac blade previously described for *H. naledi* is manifest in the Lesedi ilium, suggesting these features are present and developed from a young age.

3.2 | Analysis 1: Developmental stage

The iliac crest, AIIS, and acetabulum of the Lesedi ilium are all unfused, suggesting an age prior to adolescence, that is, under 12–14 years by recent human standards (Scheuer & Black, 2000). The AIIS appears smooth, similar to human infants and younger juveniles, and unlike the more billowed appearance of the AIIS in adolescents. Abrasion to the acetabular margins obscures whether the ischial and pubic articular strips would have had the well-developed, billowed appearance of individuals in Stage 3 or older Stage 2 juveniles. Overall size of the Lesedi ilium is comparable to human infants and small juveniles, and is smaller than immature australopiths MLD 7 and MLD 25, and subadult Sts 14 (Figure 7).

The main factors distinguishing humans in Stages 1–2 are acetabular ossification or complexity (Figure 2) and overall size (Figure 7). Because the former cannot be ascertained for the Lesedi ilium, we compared its iliac height (55.6 mm) with that of the U.W. 101-1100 mature or adult *H. naledi* from Dinaledi (79.8 mm). The Lesedi/Dinaledi proportional iliac height (0.70) falls right in the middle of the resampled distribution of proportional height of humans in Stage 2, and completely outside the range for humans in either Stages 1 or 3 (Table 4). Thus, despite its small size, given the overall size difference between *H. naledi* and modern humans (Garvin et al., 2017), the Lesedi ilium likely represents an individual who died between 4–11 years by human standards of development.

3.3 | Analysis 2: Shape affinities

We used GM to test the hypothesis that *H. naledi* retained an anatomy more similar to australopiths than to modern humans. We generated two landmark reconstructions of Lesedi using either a human or australopith template (Figure 6). Differences between these landmark reconstructions are small and do not have a meaningful impact on subsequent shape analyses (Supporting Information S1–2). Comparison of both reconstructions, whether based on only the 81 landmarks preserved on the Lesedi ilium or the full 148-landmark configuration, reveal that overall shape of Lesedi is most similar to australopiths, as measured by PD between pairs of individuals. This evidence supports our hypothesis based on the limited evidence from the Dinaledi remains. Accordingly, we present the australopith-based reconstruction of Lesedi, and analyze the full 148 landmark set for visualization purposes.

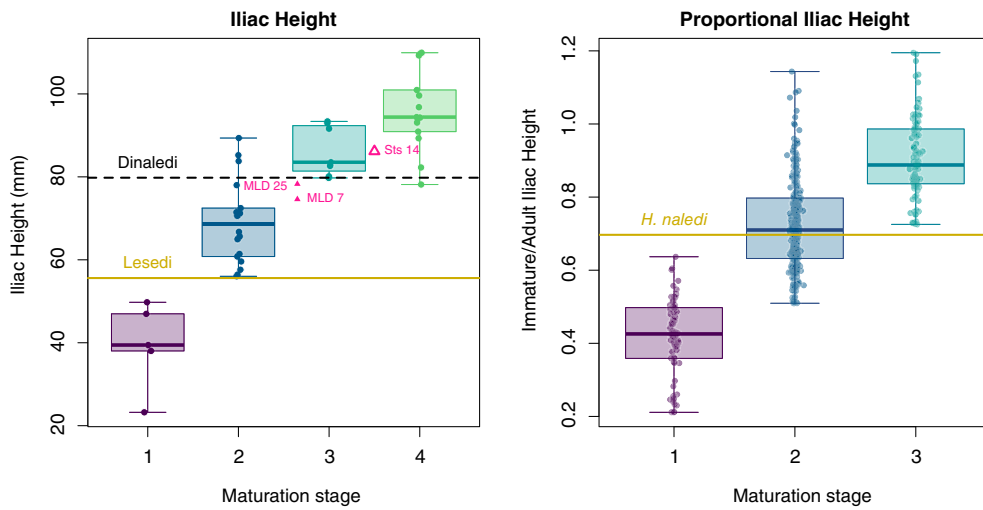


FIGURE 7 Absolute (left) and proportional (right) iliac height in modern humans, *Homo naledi* and *Australopithecus africanus*. Points in the left plot represent original individual values, while points in the right plot are resampled dyads of immature/adult individuals. The *H. naledi* line in the right plot is the proportional height of Lesedi/Dinaledi, whose original values are depicted as separate lines in the left graph. *Australopithecus africanus* subadults are depicted as pink triangles

	Mean	Standard deviation	2.5 percentile	97.5 percentile
Stage 1 (infant)	0.42	0.11	0.21	0.60
Stage 2 (juvenile)	0.71	0.13	0.52	1.02
Stage 3 (subadult)	0.91	0.11	0.73	1.17

TABLE 4 Summary of resampled proportional iliac heights

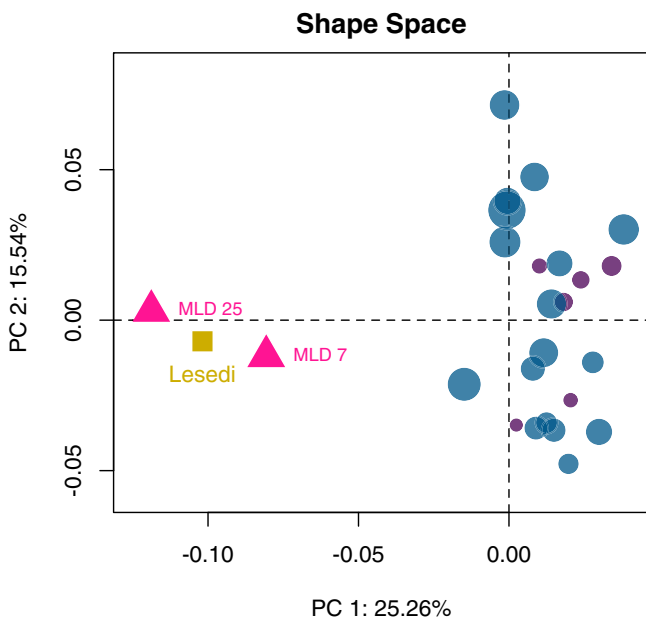


FIGURE 8 Principal component (PC) analysis of ilium shape. PCs 1–2 explain 40% of shape variation. Circles represent humans, with Stage 1 in purple and Stage 2 in navy, respectively. The size of plotted symbols is proportional to the individual's centroid size

PCA of Procrustes-aligned landmarks shows that the main axis of shape variation distinguishes humans on the one hand from Lesedi and the australopiths on the other (Figures 8 and 9). Positive PC1 scores (i.e., like humans) are associated with an anteroposteriorly elongated iliac body, expanded posterior ilium including the auricular

surface, a relatively thicker blade, a more inferiorly positioned ASIS, and more posterior or central position of the “tallest” point of the iliac crest (Figure 9): compared with the human consensus shape, the Lesedi ilium is notably similar to australopiths. This similarity is highlighted in Figure 10, depicting the Procrustes superimposition (i.e., in the same size, position, and orientation) of the Lesedi ilium, MLD 7, and the human consensus shape.

3.4 | Analysis 3: Auricular size

Despite the great overall shape similarity between Lesedi and australopiths, the superimposition in Figure 10 hints that the auricular surface of the Lesedi ilium is more similar to that of humans. Examination of auricular size, as measured by the sum of interlandmark distances along the semilandmark curve between the PIIS (Landmark 3) and superior auricular point (Landmark 7), reveals interesting patterns (Figure 11). First, the cross-sectional sample of recent humans indicates a fairly constant auricular length among Stage 1 individuals despite an overall ilium size increase, followed by commensurate increases in auricular and overall ilium size in Stage 2 (note that this plot only includes individuals with the acetabulum unfused). Second, auricular margin lengths of South African hominins are generally shorter than expected relative to immature humans of comparable size. Third, despite the smaller overall size of the Lesedi ilium, its auricular margin length is only slightly shorter than the Makapansgat australopiths, but much more similar to humans of comparable size. Importantly, this result was obtained whether using the reconstructed landmark configuration, or the lower iliac width which is better preserved in the Lesedi ilium.

FIGURE 9 Statistical shape comparisons. Top row: Ilium shapes associated with negative (orange) versus positive (navy) scores for Principal Component 1 in shape space. Bottom row: Sample mean shape (white) versus the mean shape warped to the landmark configuration of the Lesedi ilium (gold). Views from left to right are internal, external, and superior (anterior toward the top)

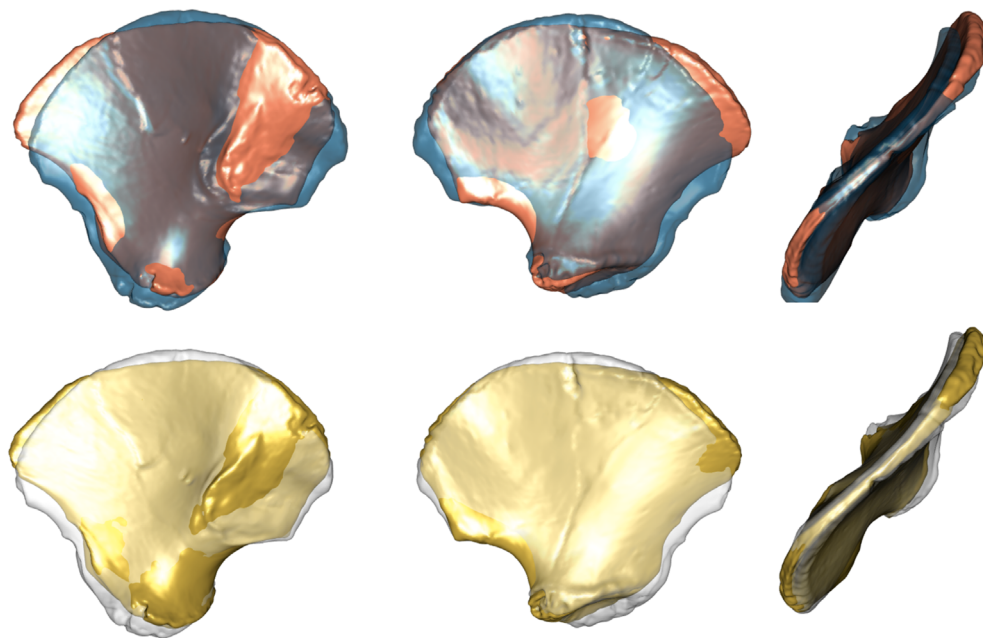


FIGURE 10 Procrustes superimposition of fossils and the human average. Left to right: Lesedi (gold) versus human average (gray); Lesedi (gold) versus MLD 7 (gray); MLD 7 (pink) versus human average (gray)

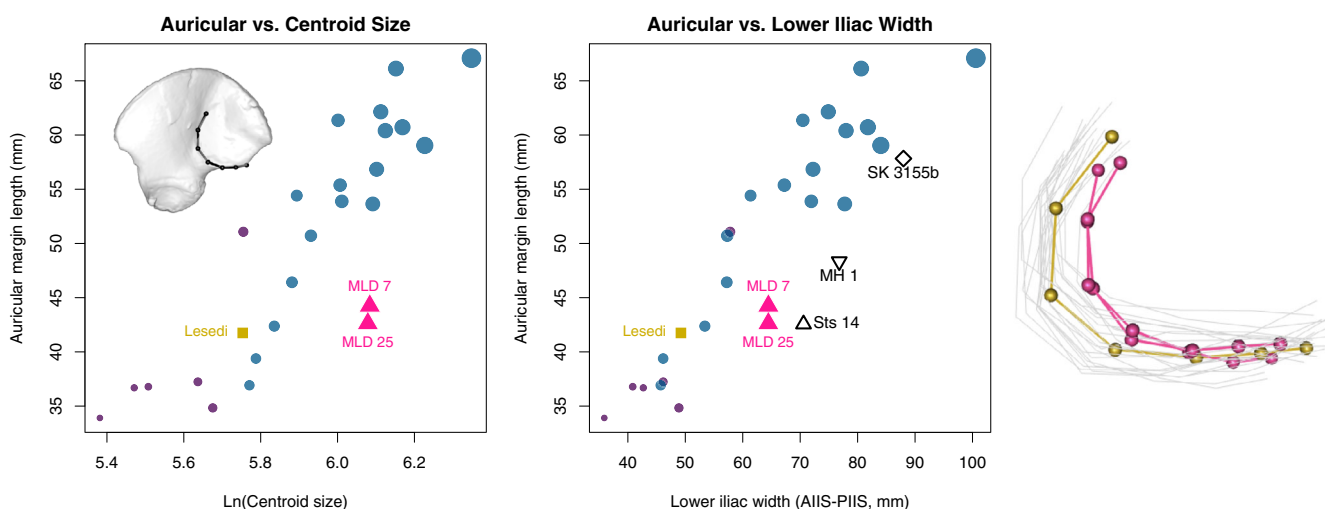
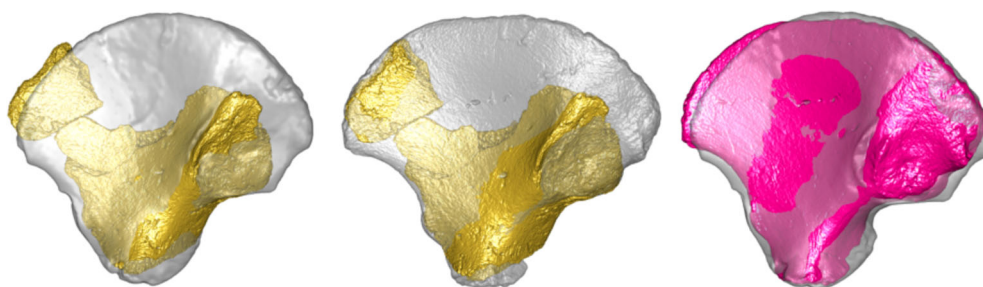


FIGURE 11 Auricular margin length plotted against Ln(Centroid size) and lower iliac width (left and center, respectively). Immature human, Lesedi, and Makapansgat data points are scaled proportional to centroid size, with point color among humans depicting Stage 1 (purple) and Stage 2 (navy). The center graph also includes South African fossils not included in the landmark-based shape analysis (black, open symbols). Right: Auricular margin outlines of immature humans (gray), *Australopithecus africanus* (pink), and Lesedi (gold), after Procrustes superimposition of complete landmark configurations

4 | DISCUSSION

Our reconstruction and analysis of the U.W. 102a–138 ilium from Lesedi confirms that *H. naledi* possessed a similar iliac blade morphology to that found in *A. africanus*, juxtaposed with an enlarged sacroiliac joint more similar to those of modern humans. It is important to acknowledge, however, that our hypothesized configuration of the U.W. 102a–138i and ii fragments is a best guess based on anatomical and geometric criteria, and the articulation between these fragments is not unequivocal. The assessment of its developmental stage based on iliac height, as well as our interpretation of an australopith-like overall ilium shape, are both dependent on our reconstruction. Corroborating the attribution to Stage 2, the AIIS of the Lesedi ilium is relatively smooth and not protuberant, in contrast to older, larger individuals in the human sample as well as the subadult australopiths MLD 7 and MLD 25. In addition, although the acetabular margin of the Lesedi ilium is abraded, there is no sign of a shelf-like rim developing near the AIIS, which again contrasts with older and larger humans as well as MLD 7, MLD 25, and MH1 (no other *H. naledi* individuals preserve this region). Thus, even if our reconstruction of the Lesedi iliac crest is incorrect, it is still probable that the individual died prior to adolescence.

We note that our human reference sample is predominated by Stage 2 individuals (Table 1), which raises the possibility of “age mimicry” affecting our results. Age mimicry is when the assessment of age-at-death is unduly influenced by the reference sample composition (Bocquet-Appel & Masset, 1982). However, we do not think that this potentially confounding factor impacts our results. First, the Lesedi ilium lacks the qualitative maturation indicators of Stage 3 individuals, as described above. In addition, the asymmetric size distribution within Stage 1 humans (Figure 7) suggests that smaller individuals are probably under-represented. A more representative Stage 1 sample would likely be more distinct from Stage 2. Finally, maturation Stage 2 itself incorporates a large proportion of the total growth period (Table 2), such that it provides too coarse a resolution to estimate age at death precisely. Future research may be able to further delineate phases of juvenile ilium development within our Stage 2 range.

Regarding the australopith-like iliac blade shape, our reconstruction was guided by several lines of evidence, drawing upon specimen preservation and referring to adult *H. naledi* from Dinaledi. The reconstruction bears a striking resemblance to MLD 7 (Figure 10), which confirms to us that it is accurate because we would not expect such close similarity if our positioning of fragments is incorrect. Furthermore, the available evidence precludes any configuration of the fragments that would yield a more human-like iliac blade. Specifically, among humans there is a relatively shorter distance between the ASIS and AIIS (e.g., Figure 9), and there is no reasonable way to position the U.W. 102a–138ii crest fragment as such. On the contrary, it is possible (but we think unlikely) that the crest fragment could be positioned further distally along the potential join with the larger 102a–138i fragment, which would produce either a more australopith-like or a uniquely long iliac blade. Thus, regardless of the uncertainty in

our reconstruction, we conclude that the iliac blade of *H. naledi* was thin, flat, and flaring, similar to australopiths. We have made surface models of these Lesedi ilium fragments available on [Morphosource.org](https://morphosource.org), for independent assessment.

A novel finding of this study is evidence for an expanded sacroiliac joint in modern human juveniles and the Lesedi ilium, compared with those of australopiths. This result is not merely an artifact of the GM reconstruction of the ilium, as we reached the same result when the auricular margin is compared with lower ilium width. The functional significance of this similarity is unclear. One possible explanation for the similarity between Lesedi and immature humans is that it reflects species differences in body size. Estimates of adult body mass for *H. naledi*, however, are comparable to those for australopiths (Garvin et al., 2017) and smaller than modern human values. Furthermore, vertebral and sacral elements of *H. naledi* are among the smallest in the hominin fossil record (VanSickle et al., 2018; Williams et al., 2017). Moreover, australopiths (Aiello & Dean, 1990; Churchill & VanSickle, 2017; Kibii et al., 2011) and many larger, adult pelvis fossils attributed to the genus *Homo* are described as having a small auricular surface (e.g., Day, 1971; Rose, 1984; Ruff, 1995; Simpson et al., 2008). As there is some ambiguity in terms of how auricular surface size is measured and compared among these various studies, an updated assessment of sacroiliac joint size in hominin evolution would be fruitful.

Another possible explanation for the enlarged sacroiliac joint of the Lesedi ilium is that *H. naledi* may have had a pattern of overall ilium growth and development distinct from either australopiths and humans; for instance, perhaps adult-like auricular size was attained at a relatively young age. Assessment of ilium development in *H. naledi*, unfortunately, requires more complete fossils than are currently available for this species (as is the case for most fossil taxa). Nevertheless, the Lesedi ilium suggests that characteristics of adult *H. naledi* were present at young ages. This is not necessarily surprising, as distinctly derived postcranial morphologies have been identified in Neandertal neonates from Mezmaiskaya and Le Moustier, for instance (Weaver et al., 2016). Making more fine-scaled assessments is more challenging. Maximum thickness of the cristal tubercle of Lesedi is about 6 mm, compared with 8 mm for the mature U.W. 101–1100 (VanSickle et al., 2018). This proportional size (0.75) is close to the proportional iliac height of Lesedi (0.70), suggesting either an isometric change, or slight proportional increase, with growth and development. In addition, the comparison of the subarcuate surface and iliac fossa between Lesedi and Dinaledi adults suggests that iliac flare may have become more accentuated with growth (e.g., Berge, 1998; Williams & Orban, 2007). Given the poor preservation of Dinaledi pelvic remains, however, it is difficult to make further inferences about ilium growth in *H. naledi* at this time.

Finally, our analyses suggest the Lesedi ilium represents an individual between ages 4–11 years by modern human standards. At this range of ages, the ilium is developmentally consistent with immature craniodental remains recovered nearby in the Lesedi Chamber (de Ruiter et al., 2019; Hawks et al., 2017). These remains include a mandible fragment (U.W. 102b–438) with a first permanent molar

that had completed alveolar emergence with incomplete root formation, and additional unerupted tooth crowns. The development of these teeth is consistent with an age of 4–6 years by human standards (Shackelford et al., 2012). The potential association of the 102b immature craniodental material with the 102a ilium, as well as undiagnosed, immature postcrania (Hawks et al., 2017), raises the possibility of an additional immature partial skeleton for *H. naledi* (cf., Bolter et al., 2020). Immature remains such as these will be critical for reconstructing growth and the pace of life history in *H. naledi* (Cofran & Walker, 2017).

ACKNOWLEDGMENTS

This research was supported by Vassar College, including the Emily Ford Fund, and both the Joan E. Morgenthau Hirschorn '44–45 Fund and Joseph H. and Florence A. Roblee Foundation. Funding for fieldwork was provided by the National Geographic Society, the Lyda Hill Foundation, the South African National Research Foundation, the South African Centre for Excellence in Palaeosciences and the LRB Foundation for Exploration. We wish to thank the Jacobs Family and later the LRB Foundation for Exploration, for access to the Rising Star site, and the South African Heritage Resource Agency and Cradle of Humankind UNESCO World Heritage Site Management Authority for issuing the various permits required for this work, including the excavation permit (PermitID: 952). We are grateful to Sifelani Jirah and Marina Elliott for access to and assistance with fossils at the University of the Witwatersrand, and to Miriam Tawane and Lazarus Kgasi for access to fossils at the Ditsong Museum of Natural History. Thanks to Marta Mirazón Lahr and Trish Biers at the University of Cambridge, and to Pedro Díaz-del-Río and Jess Beck at Consejo Superior de Investigaciones Científicas, and to Davorka Radovčić at the Hrvatski prirodoslovni muzej, for access to and assistance with comparative osteological collections. Thanks to Steve Churchill and Rebecca Cook for helpful discussion. David Katz and Barbara Fischer provided statistical advice, but we take responsibility for any errors.

CONFLICT OF INTEREST

The authors declare no conflict of interest.

AUTHOR CONTRIBUTIONS

Zachary Cofran: Conceptualization (lead); data curation (lead); formal analysis (lead); investigation (lead); methodology (lead); project administration (lead); visualization (lead); writing – original draft (lead); writing – review and editing (equal). **Caroline VanSickle:** Formal analysis (supporting); investigation (supporting); project administration (supporting); writing – original draft (supporting); writing – review and editing (supporting). **Reynaldo Valenzuela:** Formal analysis (supporting); investigation (supporting). **Daniel García-Martínez:** Formal analysis (supporting); investigation (supporting); methodology (supporting); writing – original draft (supporting); writing – review and editing (supporting). **Christopher S. Walker:** Investigation (supporting); writing – original draft (supporting); writing – review and editing (supporting). **John Hawks:** Data curation (supporting); investigation (supporting);

project administration (supporting); resources (supporting); writing – original draft (supporting); writing – review and editing (supporting). **Bernhard Zipfel:** Investigation (supporting); writing – review and editing (supporting). **Scott A. Williams:** Investigation (supporting); writing – review and editing (supporting). **Lee R. Berger:** Data curation (supporting); funding acquisition (lead); investigation (supporting); resources (supporting); writing – original draft (supporting); writing – review and editing (supporting).

DATA AVAILABILITY STATEMENT

The human skeletal remains and hominin fossils analyzed here may be accessed upon application to the respective institutions curating the collections. A 3D surface mesh of U.W. 102a-138 is available in the Morphosource repository (<https://bit.ly/2YZqKc3>). Iliac height and 3D landmark data used in this study are available in the Zenodo repository (<https://doi.org/10.5281/zenodo.5520040>).

ORCID

Zachary Cofran  <https://orcid.org/0000-0002-8688-9976>

Caroline VanSickle  <https://orcid.org/0000-0001-5338-2346>

Daniel García-Martínez  <https://orcid.org/0000-0001-7518-3866>

Christopher S. Walker  <https://orcid.org/0000-0002-5173-2784>

John Hawks  <https://orcid.org/0000-0003-3187-3755>

Scott A. Williams  <https://orcid.org/0000-0001-7860-8962>

Lee R. Berger  <https://orcid.org/0000-0002-0367-7629>

REFERENCES

- Adams, D., Collyer, M., & Kaliontzopoulou, A. (2020). *Geomorph: Software for geometric morphometric analyses (Version 3.2.1) [R package]*. Retrieved from <https://cran.r-project.org/package=geomorph>
- Aiello, L., & Dean, M. C. (1990). *An Introduction to Human Evolutionary Anatomy*. Academic Press.
- Bastir, M., García-Martínez, D., Torres-Tamayo, N., Palancar, C. A., Fernández-Pérez, F. J., Riesco-López, A., Osborne-Márquez, P., Ávila, M., & López-Gallo, P. (2019). Workflows in a Virtual Morphology Lab: 3D scanning, measuring, and printing. *Journal of Anthropological Sciences*, 97, 107–134. <https://doi.org/10.4436/JASS.97003>
- Berge, C. (1998). Heterochronic processes in human evolution: An ontogenetic analysis of the hominid pelvis. *American Journal of Physical Anthropology*, 105, 441–459. [https://doi.org/10.1002/\(SICI\)1096-8644\(199804\)105:4<441::AID-AJPA4>3.0.CO;2-R](https://doi.org/10.1002/(SICI)1096-8644(199804)105:4<441::AID-AJPA4>3.0.CO;2-R)
- Berge, C., & Gommery, D. (1999). Le sacrum de Sterkfontein Sts 14 Q (*Australopithecus africanus*): Nouvelles données sur la croissance et sur l'âge osseux du spécimen (hommage à R. Broom et J.T. Robinson). *Comptes Rendus de l'Académie des Sciences - Series IIA*, 329, 227–232. [https://doi.org/10.1016/S1251-8050\(99\)80239-0](https://doi.org/10.1016/S1251-8050(99)80239-0)
- Berge, C., & Goularas, D. (2010). A new reconstruction of Sts 14 pelvis (*Australopithecus africanus*) from computed tomography and three-dimensional modeling techniques. *Journal of Human Evolution*, 58, 262–272. <https://doi.org/10.1016/j.jhevol.2009.11.006>
- Berger, L. R., de Ruiter, D. J., Churchill, S. E., Schmid, P., Carlson, K. J., Dirks, P. H. G. M., & Kibii, J. M. (2010). *Australopithecus sediba*: A new species of *Homo*-like australopithec from South Africa. *Science*, 328, 195–204. <https://doi.org/10.1126/science.1184944>
- Berger, L. R., Hawks, J., de Ruiter, D. J., Churchill, S. E., Schmid, P., Deleuzene, L. K., Kivell, T. L., Garvin, H. M., Williams, S. A., DeSilva, J. M., Skinner, M. M., Musica, C. M., Cameron, N., Holliday, T. W., Harcourt-Smith, W., Ackermann, R. R., Bastir, M.,

- Bogin, B., Bolter, B., ... Zipfel, B. (2015). *Homo naledi*, a new species of the genus *Homo* from the Dinaledi Chamber, South Africa. *eLife*, 4, e09560. <https://doi.org/10.7554/eLife.09560>
- Bocquet-Appel, J. P., & Masset, C. (1982). Farewell to paleodemography. *Journal of Human Evolution*, 11, 321–333. [https://doi.org/10.1016/S0047-2484\(82\)80023-7](https://doi.org/10.1016/S0047-2484(82)80023-7)
- Bolter, D. R., Elliott, M. C., Hawks, J., & Berger, L. R. (2020). Immature remains and the first partial skeleton of a juvenile *Homo naledi*, a late Middle Pleistocene hominin from South Africa. *PLoS One*, 15, e0230440. <https://doi.org/10.1371/journal.pone.0230440>
- Bonmatí, A., Arsuaga, J.-L., & Lorenzo, C. (2008). Revisiting the developmental stage and age-at-death of the “Mrs. Ples” (Sts 5) and Sts 14 specimens from Sterkfontein (South Africa): Do they belong to the same individual? *Anatomical Record*, 291, 1707–1722. <https://doi.org/10.1002/ar.20795>
- Brain, C. K., Vrba, E. S., & Robinson, J. T. (1974). A new hominid innominate bone from Swartkrans. *Annals of the Transvaal Museum*, 29, 55–63. https://doi.org/10.10520/AJA00411752_217
- Churchill, S. E., Kibii, J. M., Schmid, P., Reed, N. D., & Berger, L. R. (2018). The Pelvis of *Australopithecus sediba*. *PaleoAnthropology*, 2018, 334–356. [doi/10.10520/AJA00411752_217](https://doi.org/10.10520/AJA00411752_217)
- Churchill, S. E., & VanSickle, C. (2017). Pelvic morphology in *Homo erectus* and Early *Homo*. *The Anatomical Record*, 300(5), 964–977. <https://doi.org/10.1002/ar.23576>
- Cignoni, P., Callieri, M., Corsini, M., Dellepiane, M., Ganovelli, F., & Ranzuglia, G. (2008). *MeshLab: An open-source mesh processing tool*. Paper presented at Eurographics Italian Chapter Conference. The Eurographics Association. <https://doi.org/10.2312/LocalChapterEvents/ItalChap/ItalianChapConf2008/129-136>
- Cofran, Z. D., & Walker, C. S. (2017). Dental development in *Homo naledi*. *Biology Letters*, 13(8), 20170339. <https://doi.org/10.1098/rsbl.2017.0339>
- Dart, R. A. (1949). The first pelvic bones of *Australopithecus prometheus*: Preliminary note. *American Journal of Physical Anthropology*, 7(2), 255–257. <https://doi.org/10.1002/ajpa.1330070208>
- Dart, R. A. (1958). A further adolescent australopithecine ilium from Makapansgat. *American Journal of Physical Anthropology*, 16(4), 473–479. <https://doi.org/10.1002/ajpa.1330160407>
- Day, M. H. (1971). Postcranial remains of *Homo erectus* from Bed IV, Olduvai Gorge, Tanzania. *Nature*, 232, 383–387. <https://doi.org/10.1038/232383a0>
- de Ruiter, D. J., Laird, M. F., Elliott, M., Schmid, P., Brophy, J., Hawks, J., & Berger, L. R. (2019). *Homo naledi* cranial remains from the Lesedi Chamber of the Rising Star Cave system, South Africa. *Journal of Human Evolution*, 132, 1–14. <https://doi.org/10.1016/j.jhevol.2019.03.019>
- Dirks, P. H. G. M., Roberts, E. M., Hilbert-Wolf, H., Kramers, J. D., Hawks, J., Dosseto, A., Duval, M., Elliott, M., Evans, M., Grün, R., Hellstrom, J., Herries, A. I. R., Joannes-Boyau, R., Makhubela, T. V., Placzek, C. J., Robbins, J., Spandler, C., Wiersma, J., Woodhead, J., & Berger, L. R. (2017). The age of *Homo naledi* and associated sediments in the Rising Star Cave, South Africa. *eLife*, 6, e24231. <https://doi.org/10.7554/eLife.24231>
- Fazekas, I. G., & Kósa, F. (1978). *Forensic Fetal Osteology*. Akadémiai Kiadó.
- Garvin, H. M., Elliott, M. C., Delezene, L. K., Hawks, J., Churchill, S. E., Berger, L. R., & Holliday, T. W. (2017). Body size, brain size, and sexual dimorphism in *Homo naledi* from the Dinaledi Chamber. *Journal of Human Evolution*, 111, 119–138. <https://doi.org/10.1016/j.jhevol.2017.06.010>
- Grine, F. E. (2013). The alpha taxonomy of *Australopithecus africanus*. In K. E. Reed, J. G. Fleagle, & R. E. Leakey (Eds.), *The Paleobiology of Australopithecus* (pp. 73–104). Springer. https://doi.org/10.1007/978-94-007-5919-0_6
- Gunz, P., & Mitteroecker, P. (2013). Semilandmarks: A method for quantifying curves and surfaces. *Hystrix, the Italian Journal of Mammalogy*, 24(1), 103–109. <https://doi.org/10.4404/hystrix-24.1-6292>
- Gunz, P., Mitteroecker, P., & Bookstein, F. L. (2005). Semilandmarks in three dimensions. In D. E. Slice (Ed.), *Modern Morphometrics in Physical Anthropology* (pp. 73–98). Kluwer Academic Publishers-Plenum Publishers. https://doi.org/10.1007/0-387-27614-9_3
- Halazonetis, D. (2013). *Viewbox (Version 4.0.1.7)*. Kifissia, Greece: dHAL Software. Retrieved from dhal.com
- Hawks, J., Elliott, M., Schmid, P., Churchill, S. E., Ruiter, D. J. d., Roberts, E. M., Hilbert-Wolf, H., Garvin, H. M., Williams, S. A., Delezene, L. K., Feuerriegel, E. M., Randolph-Quinney, P., Kivell, T. L., Laird, M. F., Tawane, G., DeSilva, J. M., Bailey, S. E., Brophy, J. K., Meyer, M. R., ... Berger, L. R. (2017). New fossil remains of *Homo naledi* from the Lesedi Chamber, South Africa. *eLife*, 6, e24232. <https://doi.org/10.7554/eLife.24232>
- Kibii, J. M., Churchill, S. E., Schmid, P., Carlson, K. J., Reed, N. D., de Ruiter, D. J., & Berger, L. R. (2011). A partial pelvis of *Australopithecus sediba*. *Science*, 333(6048), 1407–1411. <https://doi.org/10.1126/science.1202521>
- Kibii, J. M., & Clarke, R. J. (2003). A reconstruction of the Stw 431 *Australopithecus* pelvis based on newly discovered fragments. *South African Journal of Science*, 99, 225–226.
- Nielsen, R., Akey, J. M., Jakobsson, M., Pritchard, J. K., Tishkoff, S., & Wilerslev, E. (2017). Tracing the peopling of the world through genomics. *Nature*, 541, 302–310. <https://doi.org/10.1038/nature21347>
- Plate, T., & Heiberger, R. (2016). *abind (Version 1.4–5)* [R package]. Retrieved from <https://cran.r-project.org/package=abind>
- R Core Team. (2020). *R: A language and environment for statistical computing (version 3.6.3)* [computer software]. R Foundation for Statistical Computing. Retrieved from <https://www.R-project.org/>
- Radović, D., Cofran, Z., & Radić, D. (2018). Dental and long bone growth in four juvenile individuals from Mesolithic layers of Vela Spila Cave, Korčula, Croatia. *American Journal of Physical Anthropology*, 165(S66), 218–218. <https://doi.org/10.1002/ajpa.23489>
- Rissech, C., & Malgosa, A. (2005). Ilium growth study: Applicability in sex and age diagnosis. *Forensic Science International*, 147(2–3), 165–174. <https://doi.org/10.1016/j.forsciint.2004.08.007>
- Robbins, J. L., Dirks, P. H. G. M., Roberts, E. M., Kramers, J. D., Makhubela, T. V., Hilbert-Wolf, H. L., Elliott, M., Wiersma, J. P., Placzek, C. J., Evans, M., & Berger, L. R. (2021). Providing context to the *Homo naledi* fossils: Constraints from flowstones on the age of sediment deposits in Rising Star Cave, South Africa. *Chemical Geology*, 567, 120108. <https://doi.org/10.1016/j.chemgeo.2021.120108>
- Rosas, A., Ferrando, A., Bastir, M., García-Taberner, A., Estalrich, A., Huguet, R., García-Martínez, D., Pastor, J. F., & de la Rasilla, M. (2017). Neandertal talus bones from El Sidrón site (Asturias, Spain): A 3D geometric morphometrics analysis. *American Journal of Physical Anthropology*, 164, 394–415. <https://doi.org/10.1002/ajpa.23280>
- Rose, M. D. (1984). A Hominine Hip Bone, KNM-ER 3228, from East Lake Turkana, Kenya. *American Journal of Physical Anthropology*, 63(4), 371–378. <https://doi.org/10.1002/ajpa.1330630404>
- Ruff, C. B. (1995). Biomechanics of the hip and birth in early *Homo*. *American Journal of Physical Anthropology*, 98, 527–574. <https://doi.org/10.1002/ajpa.1330980412>
- Scheuer, L., & Black, S. M. (2000). *Developmental Juvenile Osteology*. Academic Press.
- Schlager, S. (2017). Morpho and Rvcg – Shape analysis in R. In G. Zheng, S. Li, & G. Székely (Eds.), *Statistical Shape and Deformation Analysis* (pp. 217–256). Academic Press.
- Shackelford, L. L., Harris, A. E. S., & Konigsberg, L. W. (2012). Estimating the distribution of probable age-at-death from dental remains of immature human fossils. *American Journal of Physical Anthropology*, 147(2), 227–253. <https://doi.org/10.1002/ajpa.21639>
- Simpson, S. W., Quade, J., Levin, N. E., Butler, R., Dupont-Nivet, G., Everett, M., & Semaw, S. (2008). A female *Homo erectus* pelvis from Gona, Ethiopia. *Science*, 322(5904), 1089–1092. <https://doi.org/10.1126/science.1163592>

- VanSickle, C., Cofran, Z., García-Martínez, D., Williams, S. A., Churchill, S. E., Berger, L. R., & Hawks, J. (2018). *Homo naledi* pelvic remains from the Dinaledi Chamber, South Africa. *Journal of Human Evolution*, 125, 122–136. <https://doi.org/10.1016/j.jhevol.2017.10.001>
- Ward, C. V., Feibel, C. S., Hammond, A. S., Leakey, L. N., Moffett, E. A., Plavcan, J. M., Skinner, M. M., Spoor, F., & Leakey, M. G. (2015). Associated ilium and femur from Koobi Fora, Kenya, and postcranial diversity in early *Homo*. *Journal of Human Evolution*, 81, 48–67. <https://doi.org/10.1016/j.jhevol.2015.01.005>
- Weaver, T. D., Coqueugniot, H., Golovanova, L. V., Doronichev, V. B., Maureille, B., & Hublin, J.-J. (2016). Neonatal postcrania from Mezmaiskaya, Russia, and Le Moustier, France, and the development of Neandertal body form. *Proceedings of the National Academy of Sciences of the United States of America*, 113(23), 6472–6477. <https://doi.org/10.1073/pnas.1523677113>
- Weber, G. W., & Bookstein, F. L. (2011). *Virtual Anthropology*. Springer-Verlag Wien.
- Williams, F. L., & Orban, R. (2007). Ontogeny and phylogeny of the pelvis in *Gorilla*, *Pongo*, *Pan*, *Australopithecus* and *Homo*. *Folia Primatologica*, 78(2), 99–117. <https://doi.org/10.1159/000097060>
- Williams, S. A., García-Martínez, D., Bastir, M., Meyer, M. R., Nalla, S., Hawks, J., Schmid, P., Churchill, S. E., & Berger, L. R. (2017). The vertebrae and ribs of *Homo naledi*. *Journal of Human Evolution*, 104, 136–154. <https://doi.org/10.1016/j.jhevol.2016.11.003>
- Zelditch, M. L., Swiderski, D. L., & Sheets, H. D. (2012). *Geometric Morphometrics for Biologists: A Primer*. Academic Press. <https://doi.org/10.1016/B978-0-12-386903-6.00015-0>

SUPPORTING INFORMATION

Additional supporting information may be found in the online version of the article at the publisher's website.

How to cite this article: Cofran, Z., VanSickle, C., Valenzuela, R., García-Martínez, D., Walker, C. S., Hawks, J., Zipfel, B., Williams, S. A., & Berger, L. R. (2022). The immature *Homo naledi* ilium from the Lesedi Chamber, Rising Star Cave, South Africa. *American Journal of Biological Anthropology*, 179(1), 3–17. <https://doi.org/10.1002/ajpa.24522>